Combined intra- and inter-slice motion artifact suppression in magnetic resonance imaging

Haitham M. Ahmed[a], Refaat E. Gabr[a], Abou-Bakr M. Youssef[a], Keith Heberlein[b], Xiaoping P. Hu[b] and Yasser M. Kadah[a,b1]

[a]Biomedical Engineering Department., Cairo University, Egypt
[b]Emory University/Georgia Tech Biomedical Engineering Dept., Atlanta GA 30322

ABSTRACT

We propose a technique for suppression of both intra-slice and inter-slice types of motion artifacts simultaneously. Starting from the general assumption of rigid body motion, we consider the case when the acquisition of the k-space is in the form of bands of finite number of lines arranged in a rectilinear fashion to cover the k-space area of interest. We also assume that an averaging factor of at least 2 is desired. Instead of acquiring a full k-space of each image and then average the result, we propose a new acquisition strategy based on acquiring the k-space in consecutive bands having 50% overlap going from one end of the phase encoding direction to the other end. In case of no motion, this overlap can be used as the second acquisition (NEX=2). When motion is encountered, both types motion are reduced to the same form under this acquisition strategy. In particular, detection and correction of motion between consecutive bands result in suppression of both motion types. In this work, this is achieved by utilizing the overlap area to estimate the motion, which is then taken into consideration in further reconstruction (or even acquisition if real-time control is available on the MR system). We demonstrate the accuracy and computational efficiency of this motion estimation approach. Once the motion is estimated, we propose a simple strategy to reconstruct artifact-free images from the acquired data that take into account the possible voids in the acquired k-space as a result of rotational motion between blades.

Keywords: Motion correction, magnetic resonance imaging, artifact suppression, navigator echo

1. INTRODUCTION

Accurate diagnosis in medical procedures has become widely attainable by the advent of the different medical imaging modalities. Among those, magnetic resonance imaging (MRI) is currently one of the most promising non-invasive diagnostic tools in medicine. In addition to its ability to produce anatomical images of remarkable detail and contrast, it can be used to visualize vascular structures, measure blood flow and perfusion, detect neural activation, and identify the metabolic information of different areas in the acquired images. Also, its inherently volumetric acquisition permits slices at different angles to be computed easily which can be advantageous in many applications.

One of the major problems in the present MRI technology is its susceptibility to substantial artifacts when motion occurs during the image acquisition time. Even though fast acquisition methods such as EPI and spiral imaging provide a solution to this problem for some applications, these techniques are extremely sensitive to magnetic field inhomogeneity effects as compared to regular scanning methods and have a generally low signal-to-noise ratio. This makes it difficult to accurately correlate the generated images with the physical anatomy because of geometric distortion in addition to more profound signal loss within the areas of large susceptibility mismatches. Moreover, when these imaging sequences are used in such applications as functional magnetic resonance imaging (fMRI), where a set of slices are acquired repeatedly, patient motion persists in the form of low detectability of activation sites as a result of misregistration of images along the sequences.

Due to practical constraints from the MRI machine hardware, signal-to-noise ratio, and image contrast of MRI, the imaging time commonly extends to several minutes. As a result, different parts of the collected k-space are acquired at

[1] E-mail: ymk@ieee.org

different time instants. In the ideal scenario, the imaged object does not change during the period of the experiment, and the image calculated by inverse Fourier transformation is undistorted. However, in clinical MRI setups, this scenario is not usually guaranteed because of physiological and occasional voluntary patient motion and can be even impossible to realize for moving organs such as the heart and abdominal structures. Consequently, the constructed images suffer varying degrees of distortion depending on the characteristics of the imaging sequence and the severity of motion during the scan duration.

Motion artifacts can generally be classified into either intra-slice or inter-slice motion[1,2]. The first is the result of motion in between the acquisition of different portions of the k-space while the second is the result of motion in between acquisitions of the same slice. The techniques in the literature often treated these types in completely different manners with several strategies to suppress each type independently. Given their underlying similarities, it might be advantageous to treat both problems simultaneously. In this work, we propose a new approach for suppressing motion artifacts from both types. The proposed method assumes rigid body motion and corrects for both its translational and rotational motion components without need for extra acquisitions.

2. PREVIOUS WORK

Several attempts to solve the problem of motion artifact in MRI have been reported in the literature. In general, the available techniques can be classified into four main categories. The first category attempts to suppress relative patient motion among different k-space lines within a given image through either through breath holding and chest strapping or by using cardiac and respiratory gating[3]. This minimizes the physiological component of motion between these lines at the expense of increased discomfort to the patient and/or significantly longer acquisition times. The second category uses averaging of different acquisitions to suppress the motion artifacts as well as to improve the signal-to-noise ratio of the final image. This can be done by taking the average of the corresponding k-space lines in a number of consecutive image acquisitions, or more generally by composing a weighted average of the two based on optimizing a certain objective function under given constraints[3,14]. The third category applies extra magnetic gradient lobes in the imaging sequence to eliminate the effects of motion through signal refocusing assuming a simple polynomial model for this motion[16,19]. This technique is used to minimize signal loss from moving blood and CSF within a given voxel[13]. Finally, the fourth category assumes simple forms of rigid body motion including translational and rotational components and corrects for them in a post-processing step. The motion in this category is estimated using external monitoring[20], navigator echo (only for translational motion)[1,2], symmetry constraints[9], motion periodicity constraint[4,12], or through automated techniques[5,6,10,11,15,17,18]. The effect of translational motion can be suppressed by post-processing through modifying the phase of the k-space lines according to the *a priori* knowledge about the motion[7,8,17].

In spite of the success these methods have met in some applications, they represent solutions to only a restricted class of artifacts and cannot generally be applied to more complex types of motion such as deformable body motions. Moreover, the convergence properties of automatic techniques are not generally guaranteed and therefore a general lack of robustness of these methods hindered their clinical use outside research facilities. As a result, if the patient moves significantly during the experiment, the motion artifact in the resultant images cannot be corrected. As a result, the scan has to be repeated at the expense of inefficient use of MRI machines and added discomfort to the patient. Moreover, this might not even be possible to tolerate in emergency cases. This also complicates the procedure of imaging moving organs such as the heart by adding the cardiac/respiratory gating, which again contributes to a significant prolongation of the examination time. Therefore, a technique for motion artifact suppression that does not impose any constraints on the current procedures while robustly constructing images that are free of motion artifact will have a rather profound impact on the current MRI technology and many of its clinical applications.

3. METHODS

Magnetic resonance imaging (MRI) is rapidly becoming a major modality because of its many promising and substantial capabilities for investigating various body organs, especially brain and extremities[1]. One of the problems encountered in MRI is patient movement during data acquisition, which typically takes several minutes. The motion causes artifacts in the reconstructed image, which for two-dimensional Fourier Transform (2DFT) imaging techniques appears as blurring and ghost repetitions of the moving structure. Patient motion can be classified according to its nature as rigid motion in

which all the object points undergo the same motion and non-rigid motion such as physiological movements (respiratory, cardiac). In this paper, we consider the case of rigid motion, which is commonly encountered in MR images of head, brain and limbs. First, consider the relation between the MR signal and the density distribution of the target in the imaging plane. This is given by,

$$F(k_x,k_y)=\int_{-\infty}^{\infty}\int_{-\infty}^{\infty} f(x,y)\exp[-j2\pi(k_x x+k_y y)]\,dxdy \quad , \tag{1}$$

where $F(k_x,k_y)$ is the MR signal, k_x and k_y are the spatial frequency coordinates in the readout and phase-encoding directions, respectively, $f(x,y)$ is the density distribution of the nonmoving imaging target, and x, y are horizontal and vertical coordinates in the imaging plane. In (1) it is seen that the MRI signal is the 2-D Fourier transform of $f(x,y)$. Considering the case when the k-space is acquired as consecutive bands, as in the case of segmented EPI, PROPELLER, and the proposed method, one can neglect the inter-band motion. This is true because the entire band is acquired during a single read-out period. Thus, planar rigid motion parameters during the acquisition can be regarded as a function of the band number. A planar rigid motion is the combination of translational and rotational motions. It is well known that the rotation of an object about the center of the image domain results in the same rotation of its k-space, while translational shift results in a linear phase term multiplied in the k-space[2]. Thus the effect of the motion can be written as,

$$F_d(k_x,k_y)=\exp[-j2\pi(\delta_x k_x+\delta_y k_y)].F_\theta(k_x,k_y) \ . \tag{2}$$

Here $F_d(k_x,k_y)$ is the motion-distorted MRI signal and δ_x, δ_y, and θ are the translation in the x-direction, the translation in the y-direction and the rotation angle, respectively, and $F_\theta(k_x,k_y)$ is defined as,

$$F_\theta(k_x,k_y)=F(k_x\cos\theta+k_y\sin\theta,-k_x\sin\theta+k_y\cos\theta) \tag{3}$$

The motion correction problem is that of estimating the unknown motion parameters δ_x, δ_y, and θ and using these parameters to reconstruct an artifact-free image.

Starting from the general assumption of rigid body motion, we consider the case when the acquisition of the k-space is in the form of overlapping bands of finite number of lines arranged in a rectilinear fashion to cover the k-space area of interest. We also assume that an averaging factor of at least two is desired (i.e., NEX ≥ 2), to make the inter-slice motion problem nontrivial. Instead of acquiring a full k-space of each image and then averaging the result, we propose a new acquisition strategy based on acquiring the k-space in consecutive bands having (100·(NEX-1)/NEX)% overlap going from one end of the phase encoding direction to the other end. For example, when NEX is 2, the overlap will be 50%. Fig. 1 illustrates the acquisition strategy proposed. Each band consists of a finite number of phase encoding lines acquired in a single shot so that the inter-band motion effect is limited. In case of no motion, this overlap provides the additional acquisitions required by the selected NEX value, while in the case when inter-band motion occurs, the proposed overlap provides the information that enables the determination of motion parameters as a generalization of the floating navigator echo[1].

The process of estimating the motion parameters is done in two steps: rotation estimation then 2-D translation estimation. From the geometry of the acquisition in the k-space in Fig. 1, the presence of rotation amounts to varying the area of overlap between the two consecutive bands or blades. Hence, given that this geometry is known a priori, if we compute a similarity measure between the areas of overlap at each possible rotation angle within a predetermined range of possible angles, it is possible to determine the rotation angle as the one having the highest similarity measure. We tried two different methods to do that. The first is based on a correlation coefficient between the elements in the overlapped areas to allow for the similarity measure to be independent of the size of the overlapping area. On the other hand, the second is based on matching the intensity on an arc within the overlapped area that is centered at the center of the k-space. The estimation of rotation in this method is similar to orbital navigator[7] performed on an arc instead of a circle. This approach is therefore termed arc navigator (aNAV). Points on this arc are interpolated to any desired resolution from the two acquired overlapping bands using an interpolation window like the Kaiser-Bessel window to form aNAV complex data vectors as follows:

$$aNAV(k_x,k_y)=\sum_i W(|(k_x,k_y)-(k^i_x,k^i{}_y)|)F(k^i{}_x,k^i{}_y) \tag{4}$$

where (k_x, k_y) is the point on the aNAV being interpolated and $(k^i{}_x, k^i{}_y)$ is a grid data point in the neighborhood of (k_x, k_y). $\cdot\ |(k_x, k_y) - (k^i_x, k^i{}_y)|$ is a distance measure in the 2-D space and W is the Kaiser-Bessel window and i runs over a small neighbor of the currently interpolated aNAV point. The Kaiser-Bessel interpolation window is chosen because of its good side-loop behavior[23] as well as its smoothing effect that stabilize the interpolation process in cases of low SNR. From Eq. (2) and (3), Considering only the magnitude of the k-space, we find that the effect of object rotation is to cause identical rotation of the magnitude of its k-space, hence the magnitude of the aNAV. This appears as shift in the magnitude of the aNAV data vectors and can be determined by simple correlation or in the frequency domain by fitting the phase difference between the Fourier transforms of the two aNAV signals.

It should be noted that the arc angle of an aNAV, and hence the maximum rotation captured, depends on the distance of the acquired band from the k-space origin. The closer the band from the origin, the wider its viewing angle becomes Fig. 2. The far most aNAV in an overlapping area between two bands has a viewing angle that can be determined from the location of these bands as follows,

$$\theta_{\max} = \pm \cos^{-1}((R - M/2)/R) \tag{5}$$

where R is the far most phase encoding line in the overlapped area and M is the number of phase encoding lines per band. The far most band has an arc angle of $\pm\cos^{-1}(1\text{-}M/(N\text{-}M))$ where N is the total number of phase encoding lines. For a typical image resolution of 128x128 and band size of 16, one can obtain an arc angle of at least ±31°. This allows the robust detection of a relative rotation between two consecutive bands of more than ±15° under the worst-case scenario. In cases when the SNR is too low, the strategy based on correlation coefficient is preferred in spite of its extra computational effort.

Once the rotation is determined, it is straightforward to determine the 2-D translation by fitting the phase difference between the points in the overlapped area of the aNAVs to a linear function in k_x and k_y. The phase difference $\Phi(k_x, k_y)$ is computed for each point as the phase of the complex multiplication of that point in the second band and the conjugate of the one in the first to avoid phase wrapping errors, such that,

$$\Phi(k_x, k_y) = \arg\left(aNAV_2(k_x, k_y).aNAV_1^*(k_x, k_y)\right), \tag{6}$$

where $aNAV_1$ and $aNAV_2$ are the aNAV vectors of two consecutive bands and '*' denotes the conjugate operation. This process is repeated between each two consecutive bands with correction for translational motion for the most recently acquired band. On the other hand, the rotational motion can be corrected only during the reconstruction process given the sampling non-uniformity introduced into the k-space by this type of motion. The reconstruction includes an interpolation step to calculate the k-space data on a rectilinear grid using gridding algorithms[22-25].

4. RESULTS AND DISCUSSION

The proposed algorithm was verified using simulated motion on numerical phantoms as well as images of an induced motion of a phantom obtained on a Siemens 1.5T system. The acquisition parameters were as follows: fast spin echo, TR 500ms, TE 15ms, Matrix 256x256, and ETL: 16. Fig. 2 shows a sample plot of the aNAV signals from two bands with a relative rotation of 4.5 degrees. Fig. 3 shows the arc navigator sizes and shapes for the different bands included. Figs. 4-7 show the comparison of the true and estimated motions. The apparent similarity between the curves allows for accurate estimation of the rotation angle. A wide range of motion was simulated to test the accuracy of the proposed method and simulation of noisy data was performed to test the robustness of the solution under different SNR conditions. The results indicate that the new method is capable of detecting rotations with a mean error as low as ±0.15 degrees and translation with an error that is always less than ±0.2 of the pixel width. Given that the similarity measures used implicitly average the data, the technique was found to be robust against noise in most cases. Figure 8 shows an example of motion correction on a simulated Shepp-Logan phantom using the same parameters estimated from the real data. This is to illustrate the extent of the correction on a well-known model with resolution structure. As can be seen, the correction substantially improves the resolution of the image. However, ghosting artifacts appear more prominent in the corrected

image. We believe that this is due to the resultant k-space undersampling as the result of rotation. Further investigation is needed to address this problem in depth.

5. CONCLUSIONS

A new acquisition and processing strategy was proposed to suppress both intra-slice and inter-slice motion types. The new method was implemented and verified using simulated motion on numerical phantom as well as real images and the results support the proposed hypothesis. The new technique has the advantage of not requiring additional acquisition as well as being not demanding as far as its required computational effort.

ACKNOWLEDGEMENTS

The authors would like to acknowledge support by International Electronics (Giza, Egypt), NIH (grants RO1MH55346 and RO1EB00321), Georgia Research Alliance, and The Whitaker Foundation. The authors also would like to acknowledge the use of the analytical Shepp-Logan data generator code from Ahmed S. Fahmy, The Johns Hopkins University.

REFERENCES

1. Y.M. Kadah, K. Heberlein, and X. Hu, "Floating navigator echo for in-plane translational motion estimation," *ISMRM 10 th Scientific Meetin*g, Honolulu, p. 2309, May 2002.
2. R.L. Ehman and J.P. Felmlee, "Adaptive technique for high-definition MR imaging of moving structures," *Radiology* **173**, vol. 173, pp. 255-263, 1989.
3. M.L. Wood and R.M. Henkelman, "Suppression of respiratory motion artifacts in magnetic resonance imaging," *Med. Phys.* **13**, no. 6, pp. 794-805, 1986.
4. T. Mitsa, K.J. Parker, W.S. Smith, A.M. Tekalp, and J. Szumowski, "Correction of periodic motion artifacts along the slice selection axis in MRI," *IEEE Trans. Med. Imag.* **9**, no. 3, pp. 310-317, 1991.
5. M. Hedley, H. Yan, and D. Rosenfeld, "An improved algorithm for 2-D translational motion artifact correction," *IEEE Trans. Med. Imag.* **10**, no. 4, pp. 548-553, 1991.
6. R. Steagall, S. Amartur, and E.M. Haacke, "Correcting motion artifacts via a fast, iterative, POCS procedure," *Proc. SMR Eighth Annual Meeting*, 1990.
7. H.W. Korin, F. Farzaneh, R.C. Wright, and S.J. Riederer, "Compensation for effects of linear motion in MR imaging," *Magn. Reson. Med.* **12**, pp. 99-113, 1989.
8. R.A. Zoroofi, Y. Sato, S. Tamura, H. Naito, and L. Tang, "An improved method for MRI artifact correction due to translational motion in the imaging plane," *IEEE Trans. Med. Imag.* **14**, no. 3, pp. 471-479, 1995.
9. L. Tang, M. Ohya, Y. Sato, S. Tamura, H. Naito, K. Harada, and T. Kozuka, "Artifact cancellation in MRI due to phase encoding axis motion," *Systems and Computers in Japan* **26**, no. 1, pp. 88-97, 1995.
10. M. Hedley, H. Yan, and D. Rosenfeld, "A modified Gerchberg-Saxton algorithm for one-dimensional motion artifact cancellation in MRI," *IEEE Trans. Sig. Proc.* **39**, no. 6, pp. 1428-1433, 1991.
11. M. Hedley, H. Yan, and D. Rosenfeld, "Motion artifact correction in MRI using generalized projections," *IEEE Trans. Med. Imag.* **10**, no. 1, pp. 40-46, 1991.
12. M. Hedley and H. Yan, "Suppression of slice selection axis motion artifacts in MRI," *IEEE Trans. Med. Imag.* **11**, no. 2, pp. 233-237, 1992.
13. J.L. Durek and P.M. Pattany, "Analysis of imaging axes significance in motion artifact suppression technique (MAST): MRI of turbulent flow and motion," *Magn. Reson. Med.* **7**, pp. 251-263, 1989.
14. B. Madore and R.M. Henkelman, "A new way of averaging with applications to MRI," *Med. Phys.* **23**, no. 1, pp. 109-113, 1996.
15. J.P. Felmlee, R.L. Ehman, S.J. Riederer, and H.W. Korin, "Adaptive motion compensation in MR imaging without use of navigator echoes," *Radiology* **179**, pp. 139-142, 1991.
16. P.M. Pattany, J.J. Phillips, L.C. Chiu, J.D. Lipcamon, J.L. Duerk, J.M. McNally, and Surya N. Mohapatra, "Motion artifact suppression technique (MAST) for MR imaging," *J. Comput. Assist. Tomogr.* **11**, no. 3, pp. 369-377, 1987.
17. R.A. Zoroofi, Y. Sato, S. Tamura, and H. Naito, "MRI artifact cancellation due to rigid motion in the imaging plane," *IEEE Trans. Med. Imag.* **15**, no. 6, pp. 768-784, 1996.

18. T.S. Sachs, C.H. Meyer, P. Irarrazabal, B.S. Hu, D.G. Nishimura, and A. Macovski, "The diminishing variance algorithm for real-time reduction of motion artifacts in MRI," *Magn. Reson. Med.* **34**, pp. 412-422, 1995.
19. E.M. Haacke and G.W. Lenz, "Improving MR image quality in the presence of motion by using rephasing gradients," *AJR* **148**, pp. 1251-1258, 1987.
20. X. Hu, T.H. Le, T. Parrish, and P. Erhard, ``Retrospective estimation and correction of physiological fluctuation in functional MRI," *Magn. Reson. Med.* **34**, pp. 201-212, 1995.
21. L.A. Shepp and B.F. Logan, "Reconstructing interior head tissue from X-ray transmission," *IEEE Trans. Nucl. Sci.* **NS-21**, pp. 228-236, 1974.
22. J.D. O'Sullivan, "A fast sinc function gridding algorithm for Fourier inversion in computer tomography," *IEEE Trans. Med. Imag.* **MI-4**, no. 4, pp. 200-207, 1985.
23. J.I. Jackson, C.H. Meyer, D.G. Nishimura, and A. Macovski, "Selection of a convolution function for Fourier inversion using gridding," *IEEE trans. Med. Imag.* **10**, no. 3, pp. 473-478, 1991.
24. C.H. Meyer, B.S. Hu, D.G. Nishimura, and A. Macovski, Fast spiral coronary artery imaging," *Magn. Reson. Med.* 28, pp. 202-213, 1992.
25. Y.M. Kadah, "New solution to the gridding problem," *Proc. SPIE Medical Imaging* **4684**, pp. 1-9, 2002.

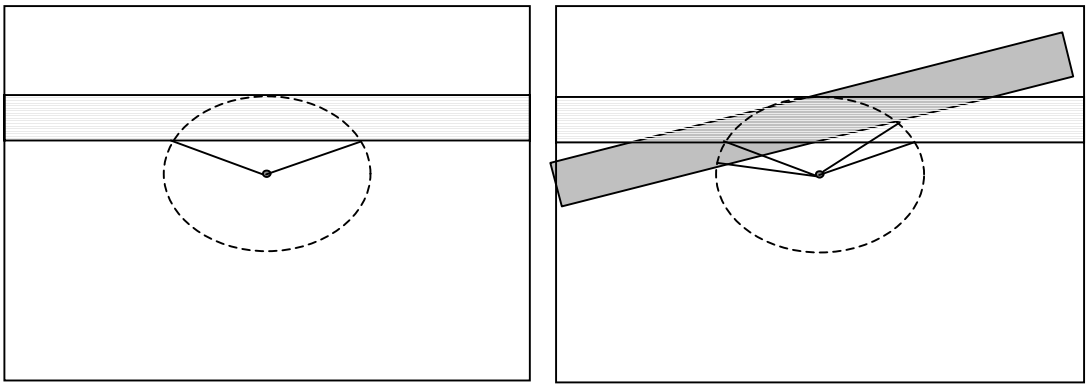

Figure 1. The overlapping area between consecutive acquisition with no motion (left) and with rotation (right) showing the aNAV position in each case.

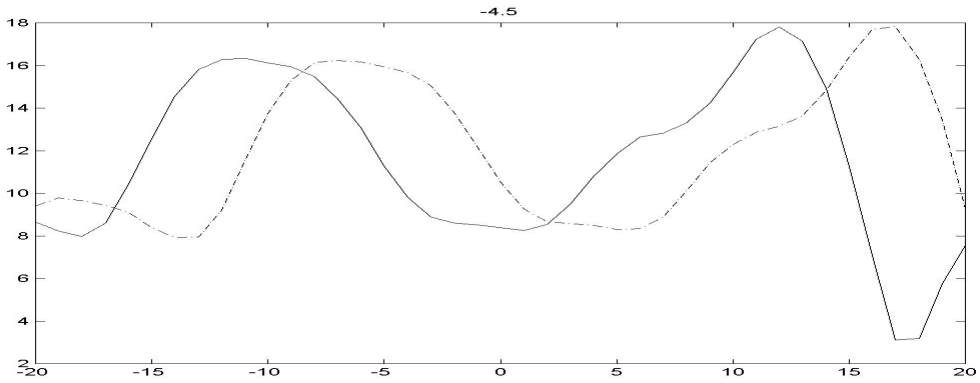

Figure 2. A plot of aNAV data for a rotation angles of 4.5 degrees showing a shift corresponding to exactly this angle.

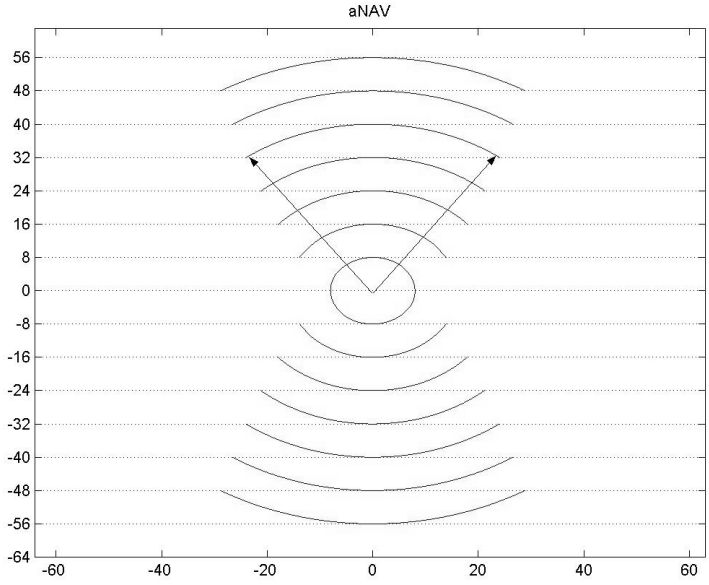

Figure 3. The change of the aNAV viewing angle with the position of subband.

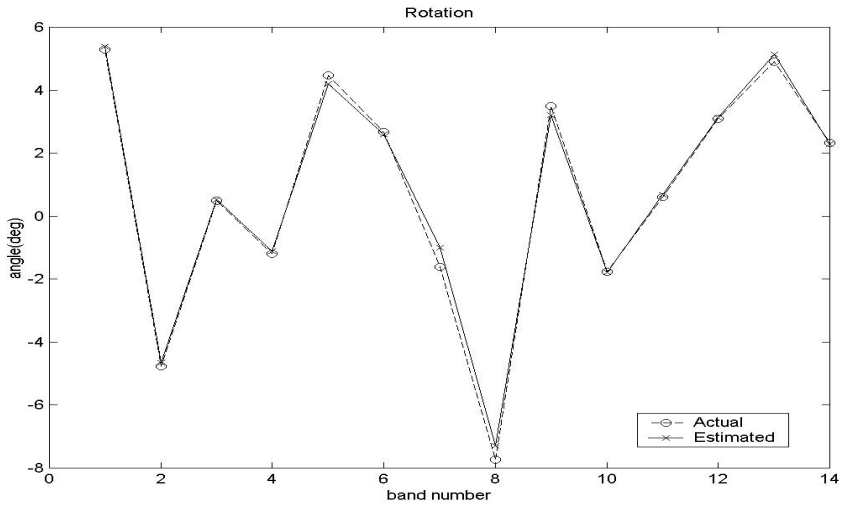

Figure 4. Angle estimated(solid) versus actual rotation angle(dashed)

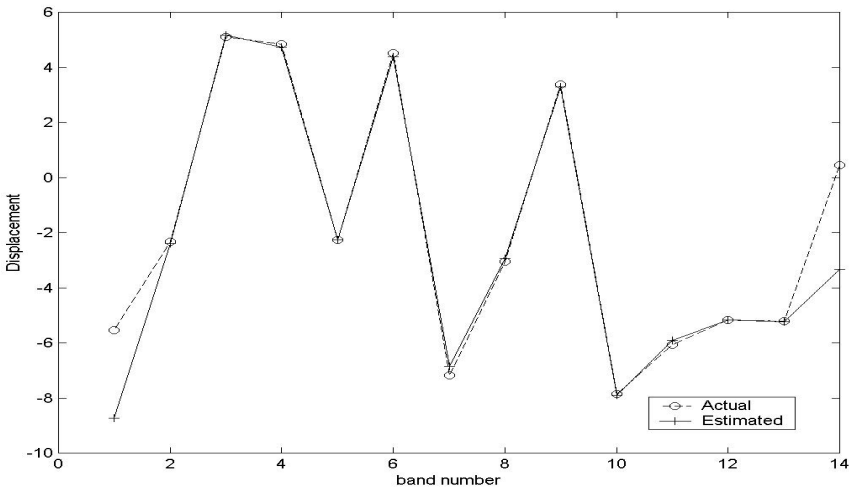

Figure 5. Read-out direction displacement estimate (solid line) versus actual displacement (dashed line)

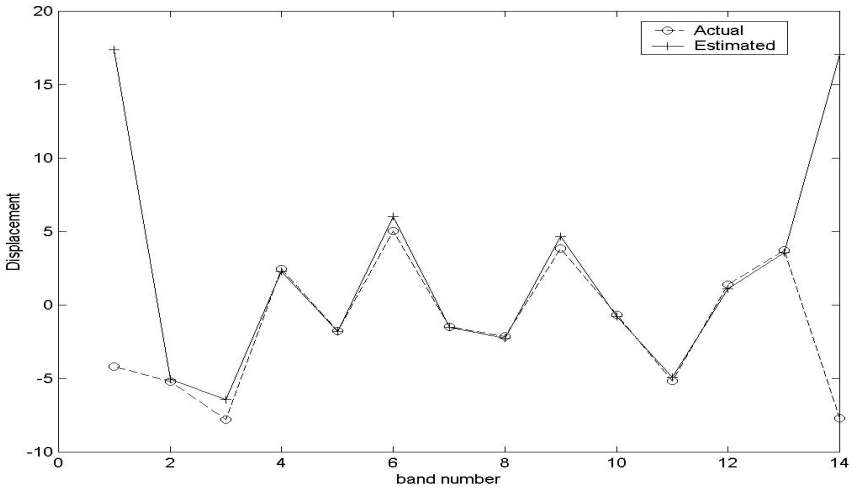

Figure 6. Phase encoding direction displacement estimate (solid line) versus actual displacement (dashed line)

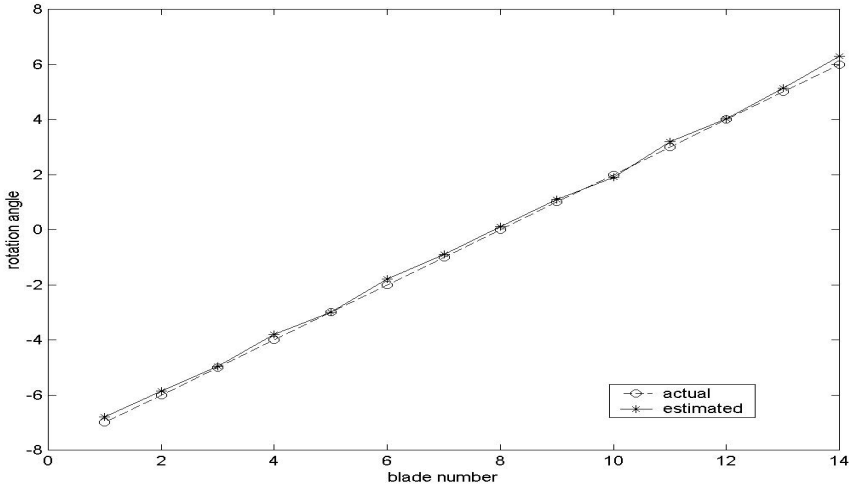

Figure 7. Estimated rotation angle (solid line) versus actual rotation angle (dashed line).

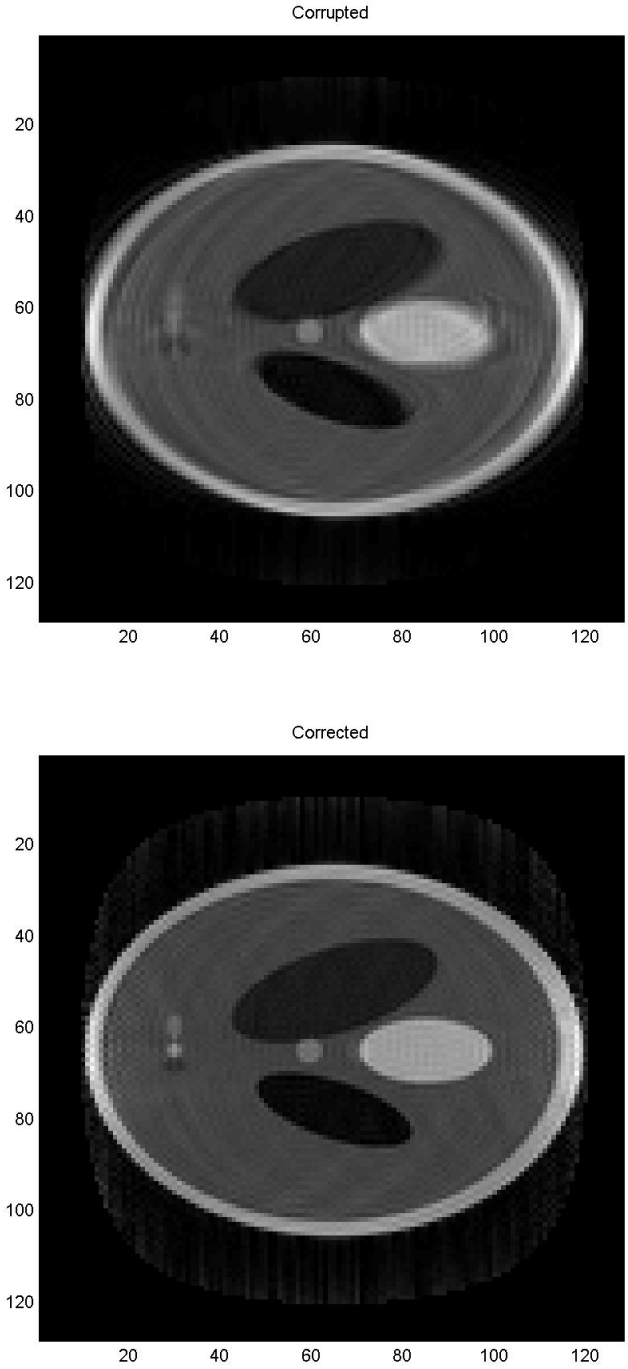

Figure 8. Simulated motion correction on a shepp-Logan phantom, motion corrupted image (top) and correction after motion estimation using the proposed technique (bottom).